

Article

Vibration Analysis of Two-Stage Helical Gear Transmission with Cracked Fault Based on an Improved Mesh Stiffness Model

Yancong Li, Shihua Yuan, Wei Wu *, Kun Liu, Chunpeng Lian and Xintao Song

National Key Laboratory of Vehicular Transmission, Beijing Institute of Technology, Beijing 100081, China

* Correspondence: wuweijing@bit.edu.cn; Tel.: +86-10-68914786; Fax: +86-10-68944487

Abstract: The crack fault has an important influence on the vibration characteristics of the transmission system. This paper is devoted to analyzing fault mechanism and dynamic characteristics of transmission with gear crack, which provides the basis for crack diagnosis and monitoring of helical gear in two-stage transmission system. For this purpose, an improved calculation method of time-varying meshing stiffness with crack fault is proposed considering the axial force of the helical gear. The influence of crack depths and angles on stiffness is analyzed. Based on this, the dynamic model of the two-stage helical gear transmission system is established using the lumped mass method. The influence of crack parameters on the characteristics of the transmission system is studied. In order to better diagnose the crack fault of the helical gear, the statistical index in time domain is calculated and the sensitivity to crack fault is analyzed. It is shown that the stiffness decreases by 25%, and the vibration acceleration increases by 8.3% after the axial force component is considered into the stiffness of the crack gear pair. The meshing stiffness decreases with the increase of crack depths and crack angles. The dynamic model is verified by rig test. Periodic impact exists in the system. The time of entering meshing of the cracked tooth and the time of complete disengagement is observed in the residual signal. In the frequency domain, there appear sidebands on the mesh frequency of the first gear pairs and its harmonics, the second gear mesh frequency and its harmonic frequencies. There is a little influence on the vibration acceleration of the driven gear of the second-stage. According to the signals in the frequency domain and the time domain, we can tell at which stage the gear is cracked. While through the time required for the crack tooth from engagement to disengagement completely, we can tell which gear is cracked. The sensitivity of skewness, impulse factor and kurtosis to crack fault decreases successively. The results provide theoretical basis for crack fault diagnosis of a two-stage helical gear transmission system.



Citation: Li, Y.; Yuan, S.; Wu, W.; Liu, K.; Lian, C.; Song, X. Vibration Analysis of Two-Stage Helical Gear Transmission with Cracked Fault Based on an Improved Mesh Stiffness Model. *Machines* **2022**, *10*, 1052. <https://doi.org/10.3390/machines10111052>

Academic Editor: Domenico Mundo

Received: 11 October 2022

Accepted: 6 November 2022

Published: 9 November 2022

Publisher's Note: MDPI stays neutral with regard to jurisdictional claims in published maps and institutional affiliations.



Copyright: © 2022 by the authors. Licensee MDPI, Basel, Switzerland. This article is an open access article distributed under the terms and conditions of the Creative Commons Attribution (CC BY) license (<https://creativecommons.org/licenses/by/4.0/>).

Keywords: crack fault; stiffness; helical transmission; dynamic model; vibration characteristics; fault diagnosis

1. Introduction

A helical gear transmission system has the characteristics of smooth transmission, strong bearing capacity and high speed. It has been widely used in aerospace, ships, automobile transportation and other fields. It is shown that gear faults account for 60% of the transmission faults [1]. Driven by motor directly, the gear working in the transmission system of pure electric vehicle bears high-frequency alternating load, which is prone to crack failure. Analysis of the vibration characteristics of cracked gear provides a theoretical basis for the diagnosis of crack fault. The accurate calculation of time-varying meshing stiffness is the key to dynamics analysis. Therefore, the calculation of helical gear meshing stiffness accurately with axial force is considered important. The influence of a crack on the vibration characteristics of a two-stage helical gear transmission system is of great significance to the fault diagnosis of helical gear.

There are several methods to calculate the stiffness of helical gears. The finite method is more accurate, but refined by the mesh accuracy, the calculation speed is relatively slow.

In some systems [2], using the analytical Hertzian model for contact deformation and FEA simulation for the bending and foundational deflection to get a more accurate stiffness in dynamic model. The analytic-FE method combines the analysis method and the finite method more accurately and saves time, but it is slightly complex for some dynamic model. The analytical method is simplified, with a lower accuracy, but it is fast. The calculation of the gear stiffness using potential energy method was proposed first by Yang and Lin [3]. In the method, the gear considered was a cantilever beam with variable cross-section. The elastic deformation of the gear included Hertz contact energy, bending deformation energy and axial compression energy. The shear deformation was also considered by Tian [4]. The foundation deformation formula was derived by Sainsot [5] and the deformation was included in the calculation of gear stiffness. In the above assumptions, the cantilever beam was from the base circle. When the root circle of the gear was larger than the radius of the base circle, the energy and deformation between the root circle and the base circle was ignored. To solve this problem, the stiffness calculation formula with a different radius of root circle and base circle was derived [6]. The error of meshing stiffness of gears with different number of teeth was reduced compared with the finite element calculation result. A cantilever beam model starting from the root circle was proposed by Ma [7] of Northeastern University. The accurate transfer curve between the tooth profile and the root circle was studied rather than considering the size relationship between the root circle and the radius of the base circle. Compared with the previous method, the calculated stiffness is closer to the finite element calculation result. After that, an improved calculation method for the helical gear was proposed [8]. With the action of axial force considered, the meshing stiffness of the helical gear was calculated [9–12]. Yan [13] calculated the meshing stiffness of the helical gear using the connection of the contact line method and the slice method. Zhang [14] calculated the meshing stiffness of helical gears using the FE-analytical slice method. Yang [15] improved the stiffness calculation of helical gears considering the flexible deflection and the clearance. Huangfu [16,17] improved the stiffness calculation method of helical gear and calculated the stiffness of helical gear with a space crack. Lin [18] studied the meshing stiffness of helical gears with crack faults.

The gear transmission system mainly consists of gears, bearings and shafts. The gear transmission system was regarded as a single degree of freedom system. Based on the impact theory, the excitation generated by the meshing impact was calculated. It was not until 1950s that the gear meshing transmission model was equivalent to the spring-mass model [19] for the first time. The one DOF model of pure torsion was established. In 1991, Kahraman and Singh [20] established a 3 DOF model considering the coupling multi-degree-of-freedom model and studied the influence of tooth clearance on it. Brethee [21] established an 8 DOF model considering the influence of motor, load and bearing. Chen [22] established the dynamics model of high-speed locomotive vehicle and gear transmission with crack faults.

Meng [23] established a dynamic model with the first-level spur gear cracked. The vibration response of the crack failure was analyzed by segmental stiffness method. Chen [24] developed the dynamic model and analyzed dynamic characteristics of a two-stage planetary gear transmission with cracked gear. The oil lubrication of bearing is analyzed in the literature [25]. An accurate dynamical model of gear systems was established [26]. Considering the eccentricity, Esayed [27] established modified helical gear models. A lumped element model was developed considering meshing stiffness and backlash [28]. Wang [29] established a distributed helical gear dynamic model with error tooth profiles. Yan [30] achieved tooth surface optimization by analyzing the dynamic characteristics of helical gears. Jiang [31] studied the helical gear dynamics model considering the friction. Wei [32] studied the calculation of time-varying meshing stiffness and dynamic characteristics of a two-stage helical gear system based on potential energy method. Liu [33] used the energy method to calculate the meshing stiffness and developed a 16 DOF model of gear-bearing-rotor using the lumped mass method.

The existing literature mainly focuses on spur gear cracks and planetary gear cracks. However, there are a few studies on the dynamics of a two-stage helical gear transmission system with crack failure considering axial force. In this paper, a calculation method of meshing stiffness of helical gear with crack fault considering the axial force and the crack fault is proposed. The lumped mass model of a two-stage helical gear transmission system with gear cracked is established. The influence of time-varying mesh stiffness and transmission error on the dynamic characteristic of gears is studied. The time-frequency signal of vibration acceleration of helical gear is obtained and compared with the experimental results. The influence of crack parameters of helical gear on vibration characteristics of the two-stage transmission system is analyzed. Considering the axial force in the stiffness model, the impact amplitude of the cracked gear vibration acceleration is 25% larger. This is helpful to realize the diagnosis of crack fault. There appears sidebands around the first mesh frequency and the second mesh frequency and their harmonics. However, the amplitude of vibration acceleration of driven gear on the output shaft changes a little when the driving gear on the input shaft is cracked.

2. Calculation of Time-Varying Meshing Stiffness of Helical Gears with Crack Fault

2.1. Computational Formula for Helical Gears with Crack Fault

Figure 1 is the force analysis diagram of helical gear. The axial force in helical gear is an important component of the meshing force, and it can be expressed as:

$$F_a = F \cos \alpha_n \sin \beta \quad (1)$$

where α_n is the normal pressure angle, β is helical gear helix angle. The method of time-varying meshing stiffness should include the axial components.

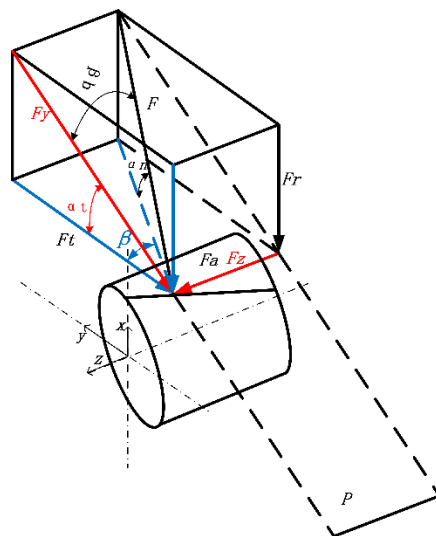


Figure 1. The force analysis diagram of helical gear.

The helical gear tooth is sliced along the tooth width, and each slice is regarded as a variable section cantilever beam. According to the theory of material mechanics and elasticity mechanics, the calculation of helical gear stiffness should include not only Hertz contact stiffness, bending stiffness caused by transverse force, shear stiffness and axial compression stiffness but also the axial bending stiffness and axial shear stiffness caused by axial force. In addition, the fillet-foundation deflection should also be included. The calculation method can be given [9] as follows:

$$dU_b = \frac{F^2}{2dk_b}, k_b = \int_0^l \frac{F^2}{2dU_b} dz \quad (2)$$

$$dU_s = \frac{F^2}{2dk_s}, k_s = \int_0^l \frac{F^2}{2dU_s} dz \quad (3)$$

$$dU_{rc} = \frac{F^2}{2dk_{rc}}, k_{rc} = \int_0^l \frac{F^2}{2dU_{rc}} dz \quad (4)$$

$$dU_{ab} = \frac{F^2}{2dk_{ab}}, k_{ab} = \int_0^l \frac{F^2}{2dU_{ab}} dz \quad (5)$$

$$dU_{as} = \frac{F^2}{2dk_{as}}, k_{as} = \int_0^l \frac{F^2}{2dU_{as}} dz \quad (6)$$

$$dU_h = \frac{F^2}{2dk_h}, k_h = \frac{EL\pi}{4(1-\nu^2)}, \quad (7)$$

where F is the meshing force, dU_b , dU_s , dU_{rc} , dU_{ab} , dU_{as} are the bending deformation energy, shear deformation energy, axial compression deformation energy, axial bending deformation energy and axial shear deformation energy of each slice, respectively. k_b , k_s , k_{rc} , k_{ab} , k_{as} , are the equivalent bending, shearing, axial compression, axial bending and axial shear stiffness, respectively. k_h is the Hertz contact stiffness, G is the shear elasticity modulus, the expression is given [34] as:

$$G = \frac{E}{2(1+\nu)} \quad (8)$$

where E is the elasticity modulus, ν is the Poisson ratio, L is the length of the contact line length.

The total energy of a slice of a pair of meshing teeth in a helical gear pair is:

$$dU = \frac{F^2}{2dk} = \frac{F^2}{2} \left(\frac{1}{dk_{b1}} + \frac{1}{dk_{s1}} + \frac{1}{dk_{rc1}} + \frac{1}{dk_{ab1}} + \frac{1}{dk_{as1}} + \frac{1}{dk_h} + \frac{1}{dk_{b2}} + \frac{1}{dk_{s2}} + \frac{1}{dk_{rc2}} + \frac{1}{dk_{ab2}} + \frac{1}{dk_{as2}} \right) \quad (9)$$

where dk is the total meshing stiffness of a slice unit, 1, 2 represents the driving gear and driven gear of the first-stage, respectively.

Besides tooth deformation, the fillet-foundation deflection also affects the meshing stiffness, so the gear fillet-foundation stiffness should be also considered [5]. The calculation method and parameter selection of fillet-foundation stiffness have been mentioned in the literature [5], so it is not described here. Therefore, the comprehensive meshing stiffness of a single pair of teeth by integrating Equation (9) is described as:

$$k = 1 / \left(\frac{1}{k_{b1}} + \frac{1}{k_{s1}} + \frac{1}{k_{rc1}} + \frac{1}{k_{ab1}} + \frac{1}{k_{as1}} + \frac{1}{k_h} + \frac{1}{k_{b2}} + \frac{1}{k_{s2}} + \frac{1}{k_{rc2}} + \frac{1}{k_{ab2}} + \frac{1}{k_{as2}} + \frac{1}{k_{f1}} + \frac{1}{k_{f2}} \right) \quad (10)$$

Figure 2 is the schematic diagram of slicing method. When more than one pairs of teeth are engaged, by adding stiffness in Equation (10), the stiffness of multiple pairs can be written as:

$$k = \sum_{i=1}^N 1 / \left(\frac{1}{k_{b1i}} + \frac{1}{k_{s1i}} + \frac{1}{k_{rc1i}} + \frac{1}{k_{ab1i}} + \frac{1}{k_{as1i}} + \frac{1}{k_{hi}} + \frac{1}{k_{b2i}} + \frac{1}{k_{s2i}} + \frac{1}{k_{rc2i}} + \frac{1}{k_{ab2i}} + \frac{1}{k_{as2i}} + \frac{1}{k_{f1i}} + \frac{1}{k_{f2i}} \right) \quad (11)$$

where the N is the number of gears engaged at the same time, i is the i th pair of gears engaged.

During the working process of helical gear, cracks may occur due to the excitation of external motor, road surface and other parts of the transmission system. With the change of meshing angle, the depth and angle of cracks will change and crack propagation will occur. As the meshing stiffness of helical gears changes, the dynamic response of gear transmission system will change.

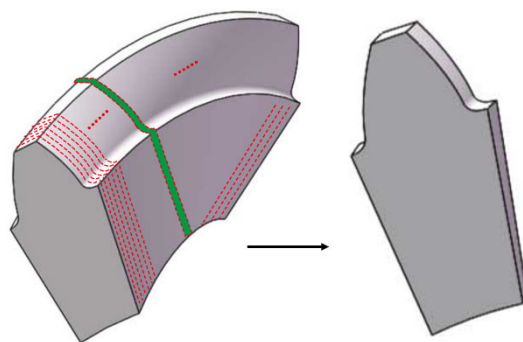


Figure 2. The schematic diagram of slicing method.

When the root crack of helical gear occurs, the bending stiffness and the shear stiffness caused by radial force, and the axial bending stiffness and the axial shear stiffness caused by axial force will change. While the axial compression stiffness caused by radial force remains unchanged, and the Hertz contact stiffness remains unchanged.

According to the relationship between the radius of the root circle and the base circle of the gear pair, the stiffness calculation of crack fault is discussed in two cases; only the process in case of $r_{b1} < r_{f1}$ is deduced in this paper.

Figure 3 is the schematic diagram of helical gear transverse face with crack fault.

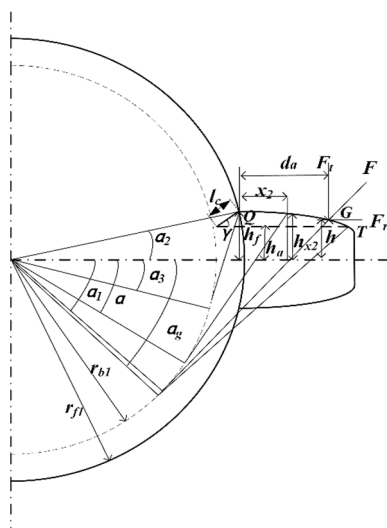


Figure 3. Schematic diagram of helical gear transverse face with crack fault.

We can see from the Figure 3 that when $r_{b1} < r_{f1}$, if the operating point of F is inside the crack affected zone, then the cross-section area is:

$$A_{x2} = \begin{cases} (h_a + h_{x2})L, & x_2 \leq d_a \\ 2h_{x2}L, & x_2 > d_a \end{cases} \tag{12}$$

where h_a is the distance from crack termination point to tooth centerline, x_2 is the distance from meshing point to root circle, d_a is the distance between the end point of the crack on the tooth and the tooth root circle, h_{x2} is the distance from the contact point to tooth centerline, and L is the contact line length. When the meshing stiffness of helical gears is calculated by slice method, the contact line length of each slice is dz . The h_a and h_{x2} are given as:

$$h_a = r_{b1} \sin \alpha_2 - l_{c1} \sin \gamma \tag{13}$$

$$h_{x2} = \begin{cases} r_{b1}[(\alpha_2 - \alpha) \cos \alpha + \sin \alpha], & 0 \leq x_2 \leq d_a \\ r_{b1}[(\alpha_2 - \alpha) \cos \alpha + \sin \alpha], & d_a \leq x_2 \leq d_t \end{cases} \tag{14}$$

where d_f is the distance from apex circle to root circle.

The inertia moment can be given by:

$$I_{x2} = \begin{cases} \frac{1}{12}(h_a + h_{x2})^3 L, x_2 \leq d_a \\ \frac{1}{12}(2h_{x2})^3 L, x_2 > d_a \end{cases} \tag{15}$$

$$I_{y2} = \begin{cases} \frac{1}{12}(h_a + h_{x2})(dz)^3, x_2 \leq d_a \\ \frac{1}{12}(2h_{x2})(dz)^3, x_2 > d_a \end{cases} \tag{16}$$

Figure 4 is the schematic diagram of a cracked gear tooth with slice method.

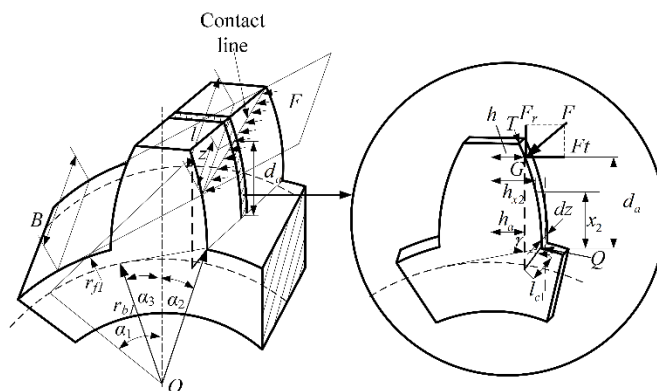


Figure 4. The schematic diagram of a cracked gear tooth with slice method.

We can see from Figure 4 that when cracks occur in helical gears, the axial compression stiffness is not affected, so the axial compression stiffness is calculated [34] by:

$$\frac{1}{dk_{rc1}} = \int_{x_Q}^{x_F} \frac{\sin^2 \alpha_n}{EA_{x2}} dx_2 \tag{17}$$

where A_{x2} is the cross-sectional area at the coordinates.

However, the bending stiffness and shear stiffness caused by radial force as well as the axial bending stiffness and axial shear stiffness caused by axial force are affected.

These parameters are put into the calculation formula of the stiffness, then we get:

$$\begin{aligned} \frac{1}{dk_{b1}} &= \int_{x_Q}^{x_F} \frac{[\cos \alpha_n \cos \beta (x_F - x_2) - \sin \alpha_n y_F]^2}{EI_{x2}} dx_2 \\ &= \int_{-\alpha_g}^{\alpha_2} \frac{[\cos \alpha_n \cos \beta \{r_{b1}(\alpha_2 + \alpha_1) \sin \alpha_1 + r_{b1} \cos \alpha_1 - r_{b1}(\alpha - \alpha_2) \sin \alpha - r_{b1} \cos \alpha\} - \sin \alpha_n (r_{b1} \sin \alpha_2 - l_{c1} \sin \gamma)]^2}{E/12(r_{b1} \sin \alpha_2 - l_{c1} \sin \gamma + r_{b1}[(\alpha_2 - \alpha) \cos \alpha + \sin \alpha])^3} r_{b1}(\alpha_2 - \alpha) \cos \alpha d\alpha \\ &+ \int_{-\alpha_1}^{-\alpha_g} \frac{\cos \alpha_n \cos \beta r_{b1}[(\alpha_2 + \alpha_1) \sin \alpha_1 + \cos \alpha_1 - ((\alpha - \alpha_2) \sin \alpha - \cos \alpha) - \sin \alpha_n r_{b1}[(\alpha_2 + \alpha_1) \cos \alpha_1 - \sin \alpha_1]]^2}{E/12(2r_{b1}[(\alpha_2 - \alpha) \cos \alpha + \sin \alpha])^3} r_{b1}(\alpha_2 - \alpha) \cos \alpha d\alpha \end{aligned} \tag{18}$$

where α_g is the involute expansion angle of the point corresponding to the crack termination point G, and it is also the critical angle of the crack affected zone. Debug the program to make the following equation in the critical condition, then we can get the critical angle α_g .

$$r_{b1}(\alpha_2 + \alpha_g) \cos \alpha_g + l_{c1} \sin \gamma = r_{b1} \sin \alpha_2 + r_{b1} \sin \alpha_g \tag{19}$$

Using the same method, the shear stiffness caused by radial force can be obtained as:

$$\begin{aligned} \frac{1}{dk_{s1}} &= \int_{x_Q}^{x_F} \frac{1.2 \cos^2 \alpha_n \cos^2 \beta}{GA_{x2}} dx_2 \\ &= \int_{-\alpha_1}^{-\alpha_g} \frac{1.2 \cos^2 \alpha_n \cos^2 \beta (1 + \nu) r_{b1} \cos \alpha (\alpha_2 - \alpha)}{E r_{b1} [(\alpha_2 - \alpha) \cos \alpha + \sin \alpha] (dz)} d\alpha \\ &+ \int_{-\alpha_g}^{\alpha_2} \frac{2 * 1.2 \cos^2 \alpha_n \cos^2 \beta (1 + \nu) r_{b1} \cos \alpha (\alpha_2 - \alpha)}{E (r_{b1} \sin \alpha_2 - l_{c1} \sin \gamma + r_{b1} [(\alpha_2 - \alpha) \cos \alpha + \sin \alpha]) (dz)} d\alpha \end{aligned} \tag{20}$$

The axial bending stiffness caused by axial force is written as:

$$\begin{aligned} \frac{1}{dk_{ab1}} &= \int_{x_Q}^{x_F} \frac{[\cos \alpha_n \sin \beta (x_F - x_2)]^2}{EI_{y2}} dx_2 \\ &= \int_{-\alpha_1}^{-\alpha_g} \frac{6 \left\{ \cos^2 \alpha_n \sin^2 \beta r_{b1}^2 [(\alpha_1 + \alpha_2) \sin \alpha_1 + \cos \alpha_1 + (\alpha_2 - \alpha) \sin \alpha - \cos \alpha]^2 \right\} (\alpha - \alpha_2) \cos \alpha}{E(dz)^3 [\sin \alpha + (\alpha_2 - \alpha) \cos \alpha]} d\alpha \\ &\quad + \int_{-\alpha_g}^{\alpha_2} \frac{12 \cos^2 \alpha_n \sin^2 \beta r_{b1}^2 [(\alpha_1 + \alpha_2) \sin \alpha_1 + \cos \alpha_1 + (\alpha_2 - \alpha) \sin \alpha - \cos \alpha]^2}{E[r_{b1}[(\alpha_2 - \alpha) \cos \alpha + \sin \alpha] + r_{b1} \sin \alpha_2 - l_c \sin \gamma] (dz)^3} r_{b1} (\alpha - \alpha_2) \cos \alpha d\alpha \end{aligned} \quad (21)$$

The axial shear stiffness caused by axial force is given by:

$$\begin{aligned} \frac{1}{dk_{as1}} &= \int_{x_Q}^{x_F} \frac{2 * 1.2 \cos^2 \alpha_n \sin^2 \beta (1 + \nu)}{EA_{x2}} dx_2 \\ &= \int_{-\alpha_1}^{-\alpha_g} \frac{1.2(1 + \nu) \cos^2 \alpha_n \sin^2 \beta}{E r_{b1} [(\alpha_2 - \alpha) \cos \alpha + \sin \alpha] (dz)} r_{b1} (\alpha_2 - \alpha) \cos \alpha d\alpha \\ &\quad + \int_{-\alpha_g}^{\alpha_2} \frac{2 * 1.2(1 + \nu) \cos^2 \alpha_n \sin^2 \beta}{E (r_{b1} \sin \alpha_2 - l_{c1} \sin \gamma + r_{b1} [(\alpha_2 - \alpha) \cos \alpha + \sin \alpha]) (dz)} r_{b1} (\alpha - \alpha_2) \cos \alpha d\alpha \end{aligned} \quad (22)$$

when the contact force is within the influence zone of the crack, the cross-section area is:

$$A_{x2} = (h_a + h_{x2})L \quad (23)$$

and the formula for calculating the moment of inertia is:

$$I_{x2} = \frac{1}{12} (h_a + h_{x2})^3 L \quad (24)$$

where L is the contact line length. When the meshing stiffness of helical gears is calculated by slice method, the contact line length of each slice is dz .

Substitute the above formula into the stiffness calculation formula of crack fault, then the bending stiffness caused by radial force is given by:

$$\begin{aligned} \frac{1}{dk_{b1}} &= \int_{x_Q}^{x_F} \frac{[\cos \alpha_n \cos \beta (x_F - x_2) - \sin \alpha_n y_F]^2}{EI_{x2}} dx_2 \\ &= \int_{-\alpha_1}^{\alpha_2} \frac{A1}{E/12(r_{b1} \sin \alpha_2 - l_{c1} \sin \gamma + r_{b1} [(\alpha_2 - \alpha) \cos \alpha + \sin \alpha])^3 (dz)} r_{b1} (\alpha_2 - \alpha) \cos \alpha d\alpha \end{aligned} \quad (25)$$

where

$$A1 = [\cos \alpha_n \cos \beta \{r_{b1} \cos(\alpha_1 + \alpha_2) \sin \alpha_1 + r_{b1} \cos \alpha_1 - r_{b1} (\alpha - \alpha_2) \sin \alpha - r_{b1} \cos \alpha\} - \sin \alpha_n (r_{b1} \sin \alpha_2 - l_c \sin \gamma)]^2 \quad (26)$$

Similarly, the shear stiffness caused by radial force is written as:

$$\begin{aligned} \frac{1}{dk_{s1}} &= \int_{x_Q}^{x_F} \frac{1.2 \sin^2 \alpha_n}{GA_{x2}} dx_2 \\ &= \int_{-\alpha_1}^{\alpha_2} \frac{1.2 \sin^2 \alpha_n (1 + \nu) r_{b1} \cos \alpha (\alpha_2 - \alpha)}{E (r_{b1} \sin \alpha_2 - l_{c1} \sin \gamma + r_{b1} [(\alpha_2 - \alpha) \cos \alpha + \sin \alpha]) (dz)} d\alpha \end{aligned} \quad (27)$$

Likewise, the bending stiffness caused by axial force can be described as:

$$\begin{aligned} \frac{1}{dk_{ab1}} &= \int_{x_Q}^{x_F} \frac{\cos^2 \alpha_n \sin^2 \beta (x_F - x_2)^2}{EI_{y2}} dx_2 \\ &= \int_{-\alpha_1}^{\alpha_2} \frac{C}{E/12[r_{b1} [(\alpha_2 - \alpha) \cos \alpha + \sin \alpha] + r_{b1} \sin \alpha_2 - l_c \sin \gamma] (dz)^3} d\alpha \end{aligned} \quad (28)$$

$$C = \left\{ \cos^2 \alpha_n \sin^2 \beta r_{b1}^2 [(\alpha_1 + \alpha_2) \sin \alpha_1 + \cos \alpha_1 - (\alpha - \alpha_2) \sin \alpha - \cos \alpha]^2 \right\} r_{b1} (\alpha - \alpha_2) \cos \alpha \quad (29)$$

The shear stiffness caused by axial force is written as:

$$\begin{aligned} \frac{1}{dk_{as1}} &= \int_{x_Q}^{x_F} \frac{2 \cdot 1.2 \cos^2 \alpha_n \sin^2 \beta (1+\nu)}{EA_{x1}} dx_2 \\ &= \int_{-\alpha_1}^{\alpha_2} \frac{2 \cdot 1.2 (1+\nu) \cos^2 \alpha_n \sin^2 \beta}{E(r_{b1} \sin \alpha_2 - l_{c1} \sin \gamma + r_{b1}[(\alpha_2 - \alpha) \cos \alpha + \sin \alpha]) (dz)} r_{b1} (\alpha_2 - \alpha) \cos \alpha d\alpha \end{aligned} \tag{30}$$

Figure 5 is the mesh stiffness of cracked gear pair when the axial force is neglected and considered, respectively. The stiffness reduced 0.7×10^8 N/m after the axial force is considered in the method. It is shown that the stiffness decreased by 25%. This is because the axial bending and the axial shear stiffness reduces when a crack fault happens.

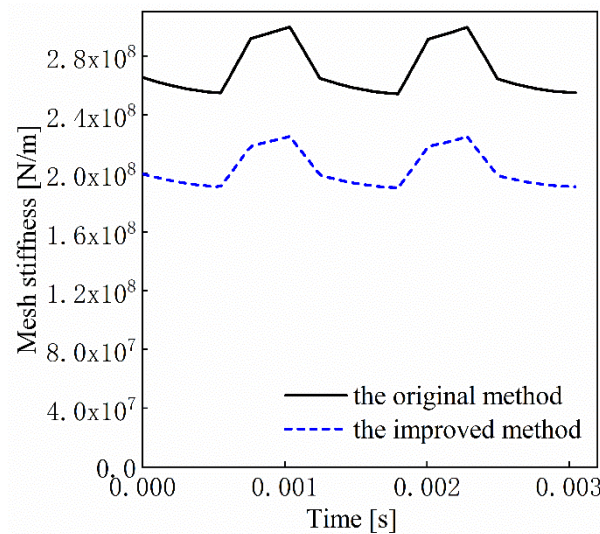


Figure 5. The mesh stiffness of cracked gear pair when axial force is considered and neglected.

2.2. Influence of Crack Parameters on the Time-Varying Meshing Stiffness

The tooth root crack of helical gear can be determined by the depth of crack on the front l_c , the crack angle γ on the front end face and crack length q . The influence of crack parameters on meshing stiffness is studied by analyzing the change of stiffness values of parameters under different values. According to the helical gear pairs listed in Table 1, the influence of parameters on time-varying meshing stiffness is analyzed. The driving gear speed is 3000 r/min. The tooth profile parameters of helical gear pair are shown in Table 1. The module is selected according to the literature [35]. The Young’s modulus and the Poission’s ratio are selected according to the value of steel in the Ansys/workbench.

Table 1. Parameters of gears.

Parameters	Driving Gear1	Driven Gear1	Driving Gear2	Driven Gear2
Number of tooth	16	52	23	71
Normal Module (mm)	1.25	1.25	1.5	1.5
Pressure angle (°)	20	20	16	16
Young’s modulus (Pa)	2.11×10^{11}	2.11×10^{11}	2.11×10^{11}	2.11×10^{11}
Poission’s ratio	0.3	0.3	0.3	0.3
Width of tooth (mm)	10	10	12	12

When the crack length q is 10 mm, the crack depth l_c of the transverse face is 2.5 mm, the stiffness is calculated. It is calculated when crack angle is 30 degrees, 45 degrees and 60 degrees, respectively. It can be seen from the Figure 6 that time-varying meshing stiffness reduces when crack fault occurred. With the increase of crack angle, the meshing stiffness of cracked gear decreases more seriously. When the crack angle is 30 degrees, the amplitude decreases by 0.1×10^7 N/m.

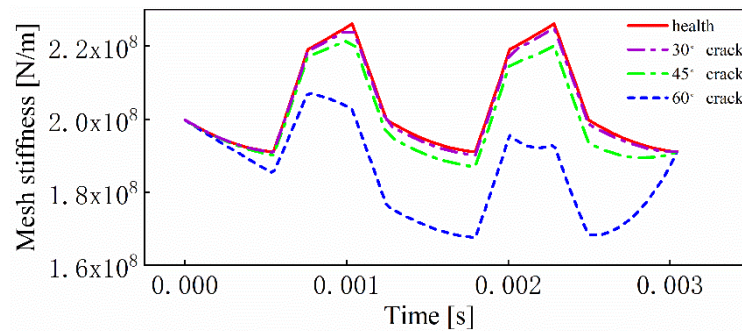


Figure 6. Stiffness values at different crack angles.

When the crack angle γ at the transverse face is 60 degrees, the influence of crack depth parameter l_c is studied with the crack length q 10 mm. The results in Figure 7 show that with the increase of crack depth, the amplitude of crack stiffness decreases more obviously. The stiffness decreases by 2.5×10^7 N/m when the crack depth is 2.5 mm. This is because the cross-sectional area and the moment of inertia reduces with the change of crack angle and depth.

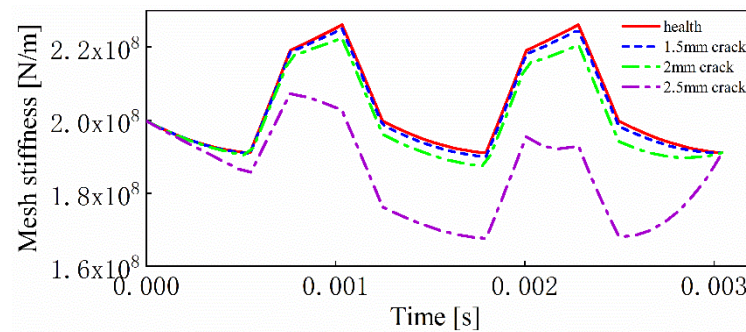


Figure 7. Stiffness values at different crack depths.

3. Establishment of Dynamic Model

y_{12}, y_{34} is the normal vibration displacement along gears 1 and 2, and gears 3 and 4, respectively, and their expressions are as follows.

$$\begin{cases} y_{12} = ((x_1 - x_{23}) \cos \alpha_t + (y_1 - y_{23}) \sin \alpha_t + r_1\theta_1 - r_2\theta_2) \cos \beta_b + (z_1 - z_{23}) \sin \beta_b - e_{12} \\ y_{34} = ((x_{23} - x_4) \cos \alpha_t + (y_{23} - y_4) \sin \alpha_t + r_3\theta_3 - r_4\theta_4) \cos \beta_b + (z_{23} - z_4) \sin \beta_b - e_{34} \end{cases} \quad (31)$$

where e_{12} is transmission error between gears 1 and 2, e_{34} is transmission error between gears 3 and 4. The expression of the two errors is written as:

$$\begin{cases} e_{12} = e_0 + e_r \cos(\omega t + \phi) \\ e_{34} = e_0 + e_r \cos(\omega t + \phi) \end{cases} \quad (32)$$

where b_{12} is the clearance between gear 1 and 2, b_{34} is the clearance between gear 3 and 4. The expressions of the displacement are:

$$f(y_{12}) = \begin{cases} y_{12} - b_{12}, y_{12} \geq b_{12} \\ b_{12}, -b_{12} \leq y_{12} \leq b_{12} \\ y_{12} + b_{12}, y_{12} \leq -b_{12} \end{cases} \quad (33)$$

$$f(y_{34}) = \begin{cases} y_{34} - b_{34}, y_{34} \geq b_{34} \\ b_{34}, -b_{34} \leq y_{34} \leq b_{34} \\ y_{34} + b_{34}, y_{34} \leq -b_{34} \end{cases}$$

The normal meshing forces between gears 1 and 2 and between gears 3 and 4 are:

$$\begin{cases} F_{12} = kf(y_{12}) + cf(\dot{y}_{12}) \\ F_{34} = kf(y_{34}) + cf(\dot{y}_{34}) \end{cases} \quad (34)$$

where F_{y12} , F_{z12} , F_{y34} , F_{z34} represents the components of contact force of gear 1 and 2 along the transverse direction and axial direction, the components of contact force of gear 3 and 4 along the transverse and axial direction, respectively, and they can be expressed as follows.

$$\begin{cases} F_{y12} = F_{12} \cos \beta_b \\ F_{z12} = F_{12} \sin \beta_b \\ F_{y34} = F_{34} \cos \beta_b \\ F_{z34} = F_{34} \sin \beta_b \end{cases} \quad (35)$$

The transmission system of pure electric vehicle is typically composed of motor, gear, bearing, elastic shaft and output half shaft of the transmission system. Therefore, a 15 DOF dynamic model of a two-stage helical gear transmission system is established in this paper, as shown in Figure 8a. In Figure 8b, T_p is the input torque of the motor, and T_g is the load torque, representing the moment of resistance to the wheel.

The model established has fifteen degrees of freedom, including the x , y , z and θ of the driving gear 1, driven gear 4, the x , y , z of the gear 2 and 3 as well as the rotation of gear 2 and gear 3. The dynamic equations are shown as follows.

The dynamics equation of the driving gear on the first level is described as:

$$\begin{cases} m_1 \ddot{x}_1 + k_{x1} x_1 + c_{x1} \dot{x}_1 = F_{y12} \cos \alpha_t \\ m_1 \ddot{y}_1 + k_{y1} y_1 + c_{y1} \dot{y}_1 = F_{y12} \sin \alpha_t \\ m_1 \ddot{z}_1 + k_{z1} z_1 + c_{z1} \dot{z}_1 = F_{z12} \\ J_1 \ddot{\theta}_1 = T_p - r_1 F_{y12} \end{cases} \quad (36)$$

The dynamics differential equation of gears on intermediate shaft is given by:

$$\begin{cases} (m_2 + m_3) \ddot{x}_{23} + k_{x23} x_{23} + c_{x23} \dot{x}_{23} = F_{y12} \cos \alpha_t - F_{y34} \cos \alpha_t \\ (m_2 + m_3) \ddot{y}_{23} + k_{y23} y_{23} + c_{y23} \dot{y}_{23} = F_{y12} \sin \alpha_t - F_{y34} \sin \alpha_t \\ (m_2 + m_3) \ddot{z}_{23} + k_{z23} z_{23} + c_{z23} \dot{z}_{23} = F_{z1} - F_{z2} \\ J_2 \ddot{\theta}_2 = F_{y12} r_2 - (c_{23}(\dot{\theta}_2 - \dot{\theta}_3) + k_{23}(\theta_2 - \theta_3)) \\ J_3 \ddot{\theta}_3 = (c_{23}(\dot{\theta}_2 - \dot{\theta}_3) + k_{23}(\theta_2 - \theta_3)) - F_{y34} r_3 \end{cases} \quad (37)$$

The dynamics differential equation of gear on output shaft is written as:

$$\begin{cases} m_4 \ddot{x}_4 + k_{x4} x_4 + c_{x4} \dot{x}_4 = F_{y34} \cos \alpha_t \\ m_4 \ddot{y}_4 + k_{y4} y_4 + c_{y4} \dot{y}_4 = F_{y34} \sin \alpha_t \\ m_4 \ddot{z}_4 + k_{z4} z_4 + c_{z4} \dot{z}_4 = F_{z34} \\ J_4 \ddot{\theta}_4 = r_4 F_{y34} - T_g \end{cases} \quad (38)$$

where x , y , z , respectively, represents the displacement in three directions, and the subscripts represent gears 1 to 4. θ is the torsional degree, p , g represents the driving and the driven gear, α_t is the end pressure angle of helical gear. The parameters selected of the system are shown in Table 2.

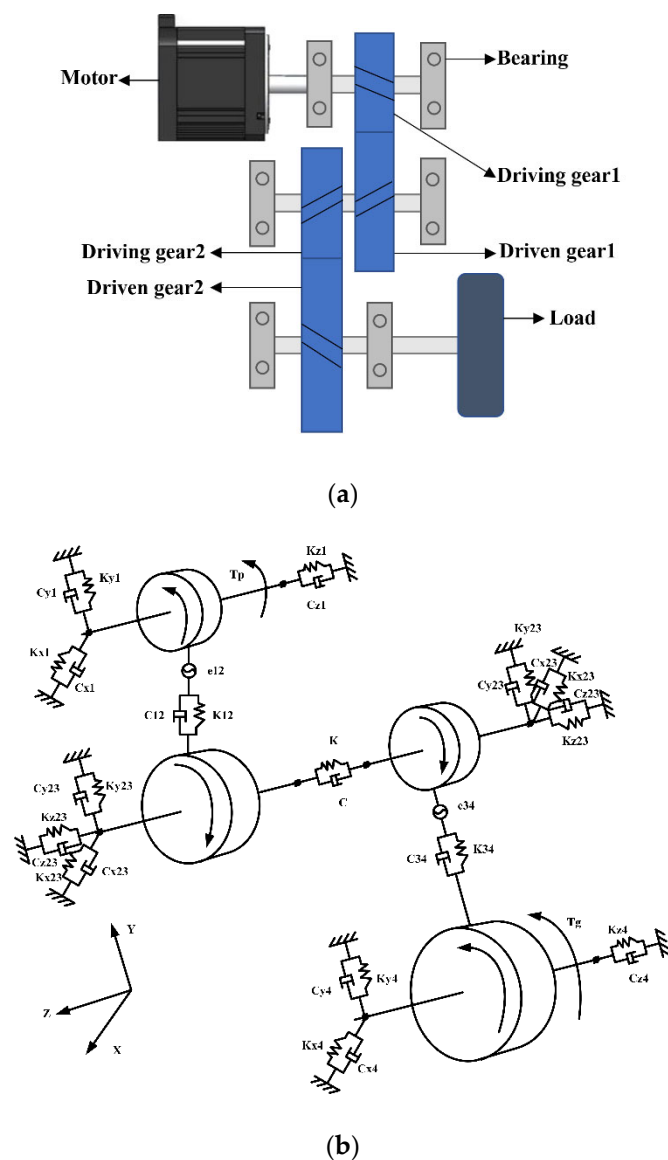


Figure 8. The two-stage drive system. (a) The physical model. (b) The dynamic model.

Table 2. Stiffness and damping parameters used in the transmission system.

Parameters	Value	Unit
$k_{xi}, i = 1, 23, 4$	8×10^7	N/m
$k_{yi}, i = 1, 23, 4$	8×10^7	N/m
$k_{zi}, i = 1, 23, 4$	5×10^7	N/m
$k_i, i = 1, 23, 4$	1.2×10^5	N.m/rad
$c_{xi}, i = 1, 23, 4$	500	N/(m/s)
$c_{yi}, i = 1, 23, 4$	500	N/(m/s)
$c_{zi}, i = 1, 23, 4$	500	N/(m/s)
$c_i, i = 1, 23, 4$	10	N.m/(rad/s)

4. Analysis of Dynamic Characteristics of Transmission System

4.1. Experimental Test

Figure 9 is the test of the two-stage transmission system. A two-stage electric drive system test platform is built, as shown in Figure 9a. The system consists of driving motor, two-stage helical gear reducer, half shaft, torque speed sensor, loading motor, controller, accelerometer and so on. The transmission system parameters used are shown in Table 1.

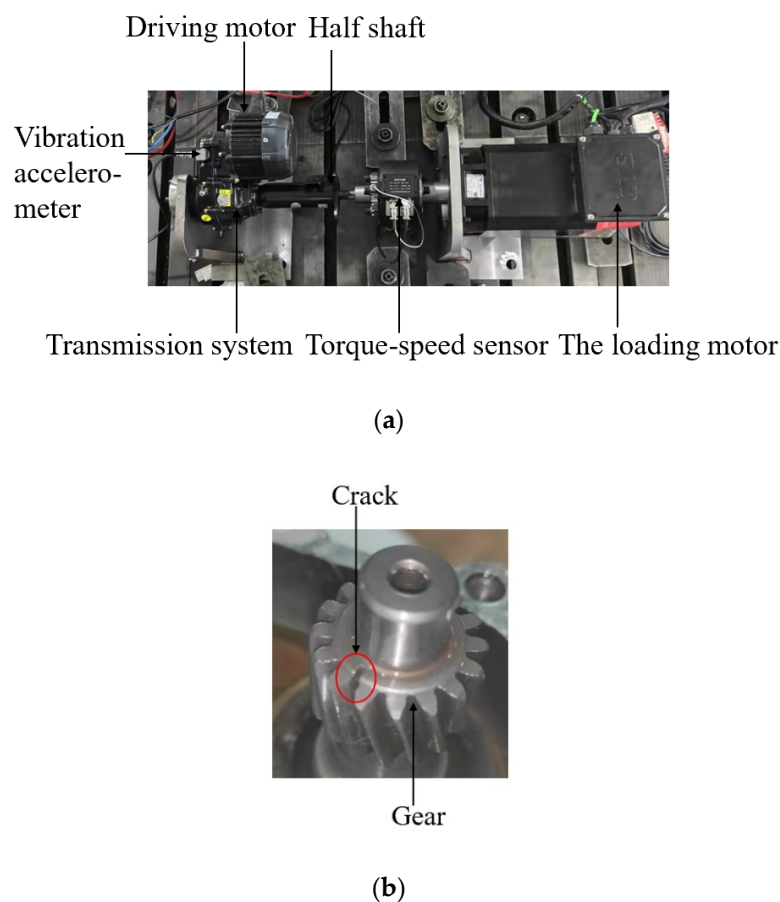


Figure 9. The test rig. (a) The helical gear test rig. (b) The gear with crack fault.

The accelerometer SAE30001 made in Shi'ao Technology is used in this system. The voltage sensitivity is 500 Mv/g. The vibration accelerometer is installed at the bearing of the two-stage drive system near the first driving gear on the gearbox. The sampling frequency of the accelerometer used is 40 kHz. After working for 10 min, with the system working stably, data is sampled for approximately 2 min.

A 10 N.m torque is applied to the transmission system. The motor input speed is set as 3000 rpm, the same parameters as the simulated. The vibration acceleration data is obtained in the upper computer.

4.2. Analysis of the Simulation and Test Result

The dynamics model of the transmission system established in the above part is solved using Runge-Kutta method. The improved method is used to calculate the stiffness of the gear with crack fault and the gear under normal state. The calculated stiffness is used in the dynamics model.

It is assumed that a crack fault occurs on a tooth of a high-speed driving gear in the transmission system, with the parameters of 10 mm length, 2.5 mm depth, and 30 degrees angle. Figure 10 shows the test and simulated result under normal state in time domain. There appears regular vibration in the test and simulated vibration, and there is no obvious impact in the vibration.

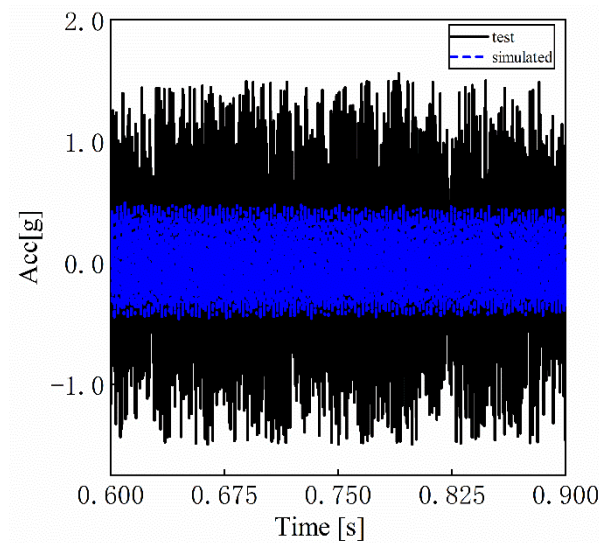


Figure 10. Time domain diagram of vibration acceleration of the helical gear in normal state.

Figure 11 is the test and simulated vibration result under healthy state in the frequency domain. Fourier transform is applied to the experimental and simulated acceleration in time domain. Then, we get the data in frequency. The blue line represents the simulated acceleration vibration, and the red line represents the test data. There are mesh frequency f_{m1} of the first gear pairs, mesh frequency f_{m2} of the second gear pairs, the harmonic frequencies of the mesh frequency $2f_{m1}$, $3f_{m1}$, and $4f_{m1}$ in the frequency domain under normal state. The amplitude at harmonic frequencies is smaller than that of the gear mesh frequency f_{m1} and f_{m2} . The simulated result is consistent with the test data. This indicates that the dynamic model is correct.

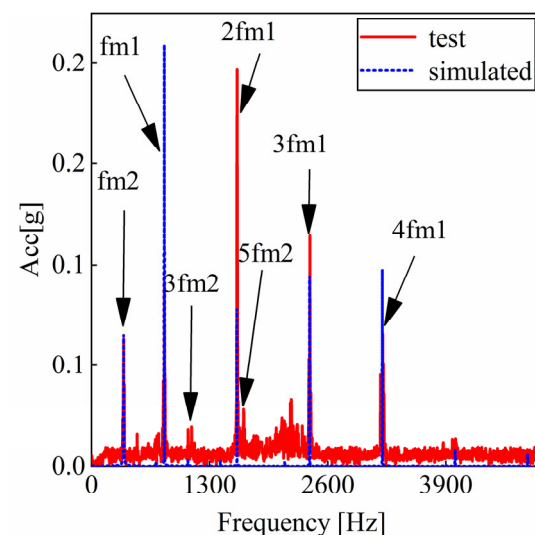


Figure 11. Frequency domain diagram of vibration acceleration of the helical gear in normal state.

5. Dynamic Characteristics Analysis of Transmission System with Crack Fault

5.1. Influence of the Crack on Vibration Response of Transmission System

Figure 12 shows the test and simulated result of the first gear under fault state. The blue line is the simulated acceleration vibration in time domain, and the black line represents the test acceleration vibration. Choosing 0.3 s as the analytical time, there is a small deviation between the simulated signal and the test data. This is because there is a small deviation of starting time between the simulated data and the test data. There appear regular impacts in the test and the simulated vibration, and the time T is the rotation frequency. This is the time

of the input shaft rotating a cycle. In time domain, the result of the simulated is consistent with the test data. The amplitude of vibration is larger than that under normal state.

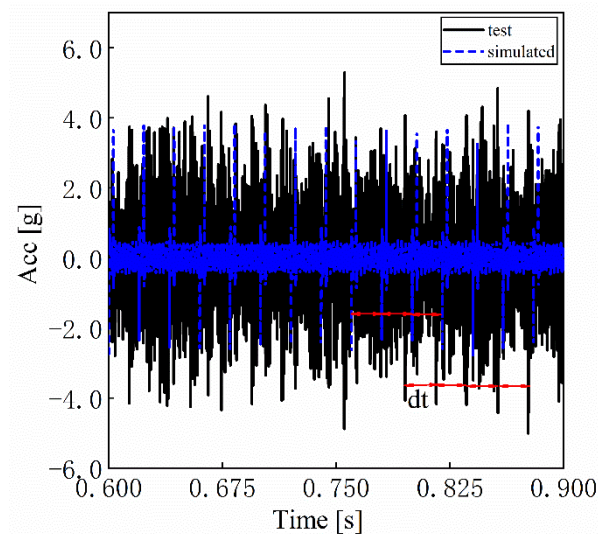


Figure 12. Time domain diagram of vibration acceleration of the helical gear in faulty state.

In order to analyze fault signals more clearly, the difference between vibration acceleration in faulty state and that in normal state in time domain is defined as the residual signal. Figure 13 is the result of residual vibration acceleration under cracked state over time. The depth of the crack is 2.5 mm and the crack angle is 30 degrees. In Figure 13, T is 0.02 s, which is the time for a gear rotating a cycle. It is also the rotation period of the shaft the cracked gear located on. This indicates that the periodic impact vibration is caused by the crack fault. The impact amplitude is approximately 3 g. T_c is 0.0030431 s, which is the time required for the crack tooth from engagement to disengagement completely. The $t1$ represents the time one gear rotating from the tooth after the cracked one. Working to the time $t2$, the cracked tooth starts to enter mesh. After the time T_c , the cracked tooth disengages completely. Then, the tooth after the cracked one enters meshing, starting the next cycle from the time $t3$. Telling the impact time, we can deduce which gear is faulty in the two-stage helical system.

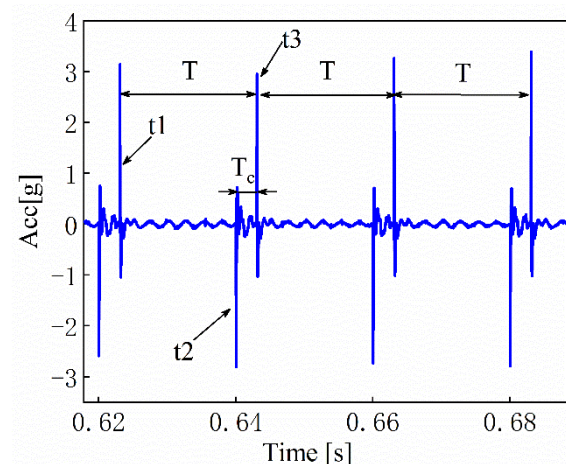


Figure 13. Residual vibration acceleration under cracked state over time.

Figure 14 is the vibration result in frequency domain. Fourier transform is applied to the test and simulated data in time domain data in Figure 12. The red line represents the test acceleration in frequency domain, and the blue represents the simulated result. There

appears sidebands around the frequency of the mesh frequency and its harmonics, and the zoomed plot is shown in Figure 15. The sideband frequency is the rotation frequency of the shaft mounting the faulty gear.

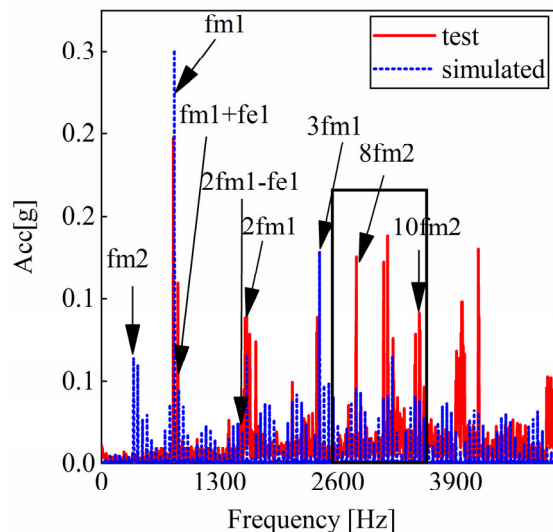


Figure 14. Frequency domain diagram of vibration acceleration of the helical gear in faulty state.

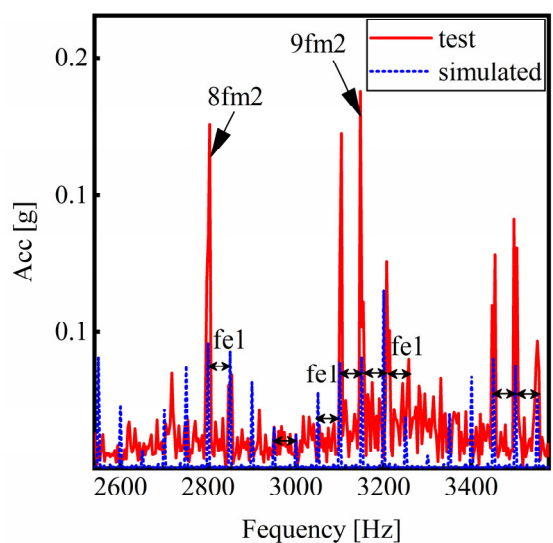
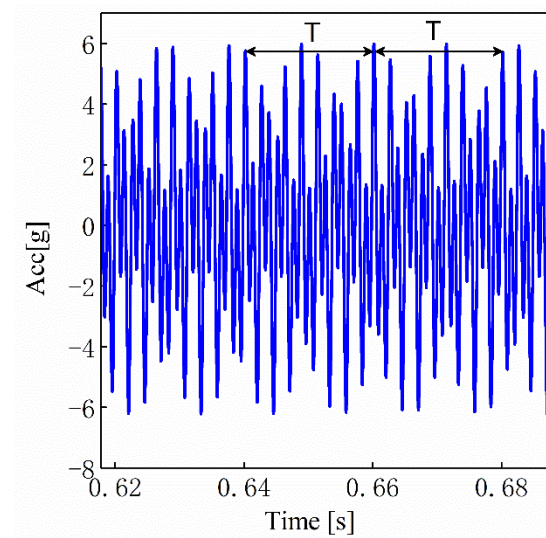


Figure 15. The zoomed plot of Figure 14.

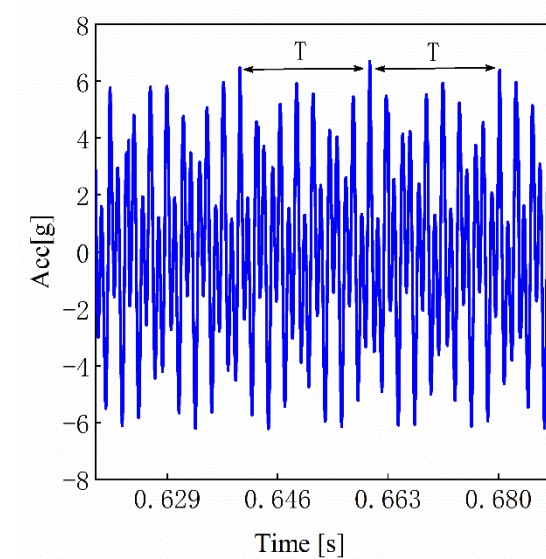
5.2. Influence of the Stiffness Considering Axial Force on Vibration Response with Cracked Fault

The vibration acceleration of the driving gear 1 over time in y-direction under the cracked condition is shown in Figure 16. The gear is cracked with the crack depth of 2.5 mm and the crack angle of 30 degrees. Figure 16a is the vibration acceleration over time with axial force neglected. The amplitude of the impact vibration is less than 6 g. Figure 16b is the vibration acceleration over time considering the axial force. From the Figure 16b, we can see that there are obvious periodic impacts. The amplitude of these impacts increases to more than 6 g, larger than that without considering the axial force. The period of the impacts is T . The T equals to the time used by the shaft mounting the faulty gear to rotate a cycle. The impact characteristics caused by faults in time-domain Figure 16b are more obvious compared with those in Figure 16a. The vibration acceleration increases by 8.3% after the axial force is considered into the stiffness of the crack gear pair. This indicates that the characteristics of the crack fault are more obvious after considering the axial force. This is helpful for the diagnosis of crack faults. The increased impact amplitude suggests

that the difference between the stiffness in cracked status and the stiffness under normal status is bigger than compared with the method without considering the axial force. This is because bending stiffness and shear stiffness are reduced due to the crack fault without considering the stiffness calculation of axial force, while with the axial force considered, the deformation resulted by the axial force increases, resulting in the reduction of the axial bending stiffness and axial shear stiffness in addition to the reduction of the bending stiffness and shear stiffness.



(a)



(b)

Figure 16. Vibration acceleration under cracked state. (a) Before improved. (b) After improved.

The acceleration of the gear on the output shaft of the two-stage gears under the healthy and the faulty state is analyzed in Figure 17. Fourier transform is applied to the vibration acceleration of the driven gear 4 in x direction in time domain. The influence of the crack fault is small on the second gear of the output shaft. The acceleration vibration amplitude of the driven gear of the second-stage at the mesh frequency is reduced only approximately 0.08 g. There is nearly no sidebands around the mesh frequency and its harmonics.

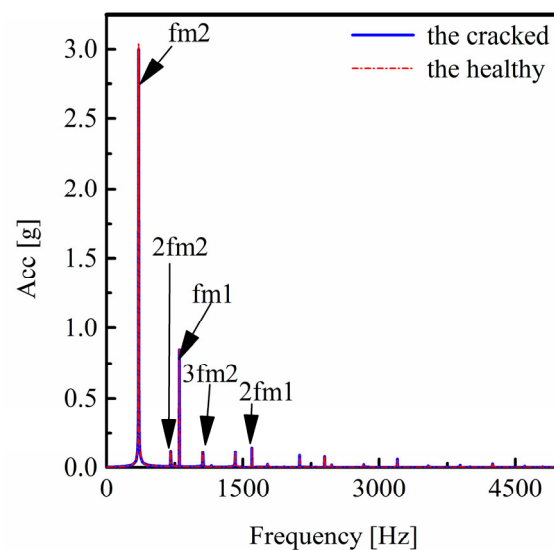


Figure 17. Frequency domain diagram of vibration acceleration of the driven gear in second stage under faulty state.

5.3. Influence of Transmission Error on Vibration Response of Transmission System

The vibration acceleration over time with different transmission errors under normal state is shown in Figure 18. The blue, green and red lines represent the vibration acceleration in the y direction in normal state with the 0 error amplitude, 20 μm error amplitude and 50 μm error amplitude, respectively. It can be seen from Figure 18 that the vibration amplitude with the three errors is approximately 0.5 g, 4 g and 12 g, respectively. With the increase of the transmission error, the vibration acceleration amplitude increases significantly.

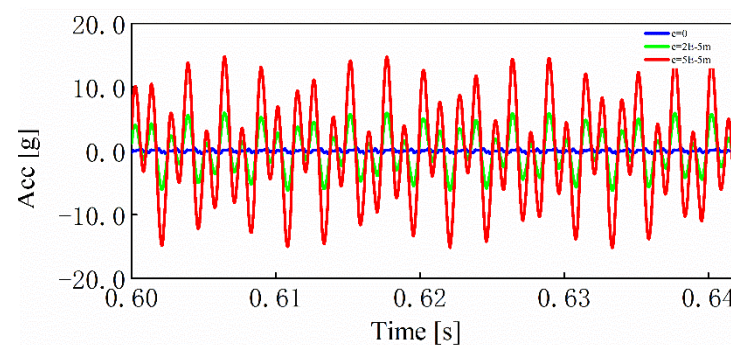
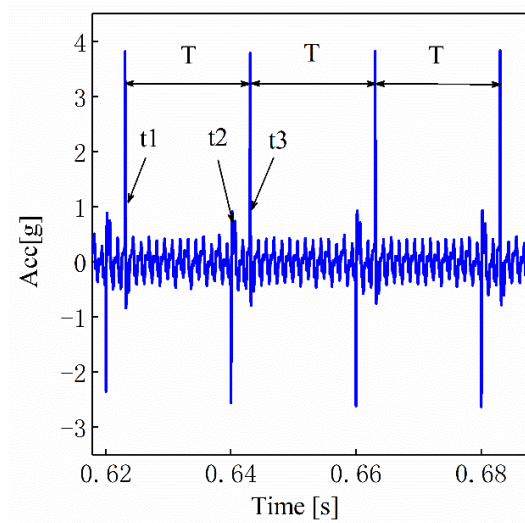
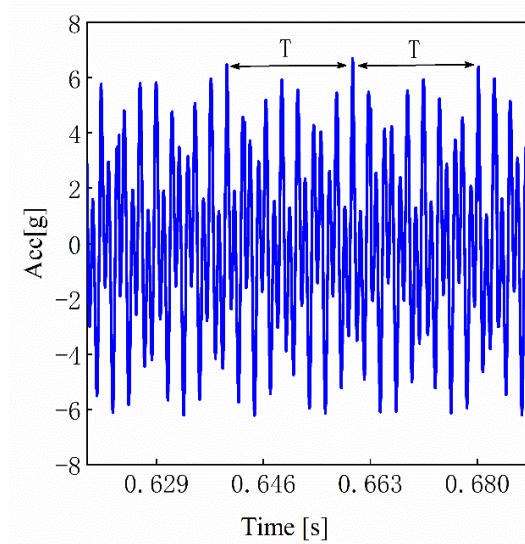


Figure 18. Time domain diagram of vibration acceleration under different transmission errors.

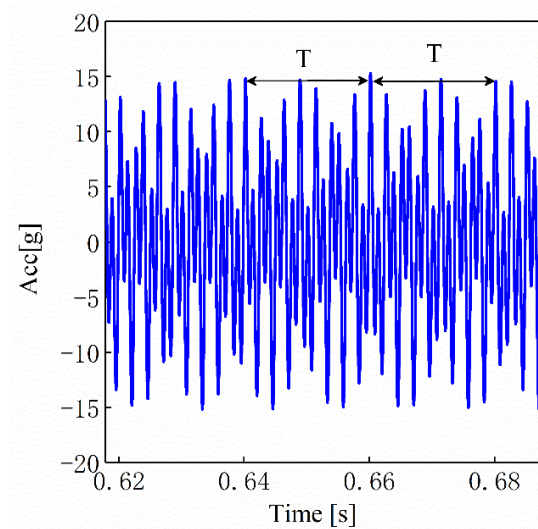
Figure 19 is the acceleration signal of gearbox with different transmission errors under faulty condition. Figure 19a shows the vibration acceleration of a cracked gear with the crack depth of 2.5 m, the crack angle of 30 degrees and the crack length of 10 mm when the transmission error amplitude $e = 0$. The periodic vibration impact caused by the fault can be clearly observed in Figure 19a. The cracked gear starts entering meshing at the moment t_2 , and at the moment t_3 , the cracked gear disengages completely. Figure 19b shows the vibration acceleration when e equals to 20 μm . The amplitude is approximately 4 g. Periodic impact exists, but it is not obvious as that when e is 0. Figure 19c is the vibration acceleration over time when e is 50 μm , and its amplitude is 12 g. The periodic impact is not obvious. It shows that the vibration amplitude increases with the increase of transmission error amplitude e , which is consistent with the conclusion in a normal state. However, the periodic impact characteristics caused by crack faults are submerged heavily, increasing the difficulty of the crack fault diagnosis.



(a)



(b)



(c)

Figure 19. The acceleration of the gear with crack fault under different transmission error amplitudes. (a) $e = 0$. (b) $e = 20 \mu\text{m}$. (c) $e = 50 \mu\text{m}$.

5.4. Influence of Different Crack Parameters on Vibration Response of Transmission System

The vibration characteristics of the transmission system under different crack angles and different crack depths are analyzed. In order to make the crack fault characteristics more obvious, the difference between the vibration acceleration value under faulty state and that under normal state is defined as the residual signal. This signal reduces the interference of the transmission error on the crack fault characteristics. The residual errors of residual errors of gear vibration acceleration at different crack angles over time is shown in Figure 20. The red, green and blue lines show the residual signals of 30 degrees crack, 45 degrees crack and 60 degrees crack with the crack depth 2.5 mm and the tooth length 10 mm (100% gear root width). Figure 20a shows that there exists obvious vibration impact characteristics at the three angles, and the impact amplitude is approximately 3 g. In zoomed plot Figure 20b, it can be seen that the impact amplitude increases as crack angle increases.

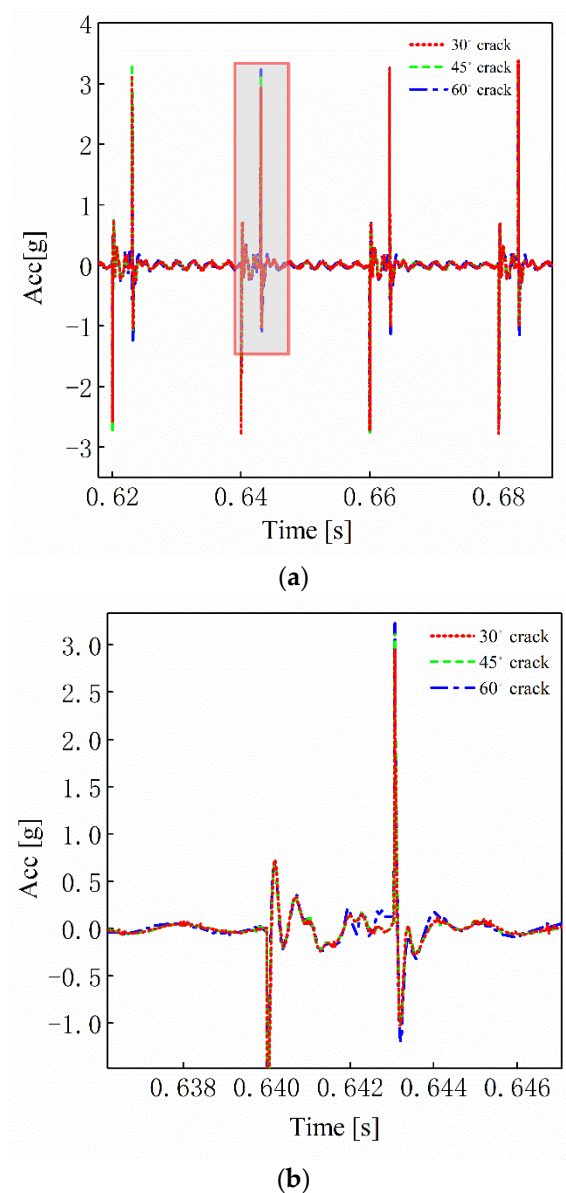


Figure 20. Time-domain diagram of residual error of vibration acceleration at different crack angles. (a) The whole. (b) Zoomed plot.

Figure 21 is the residual signals of vibration acceleration at different crack depths. Red, green and blue lines represent the residual signal of the 1.5 mm depth crack, 2 mm

depth crack and 2.5 mm depth crack over time when the crack length of the root crack is 10 mm, and the crack angle is 60 degrees. Figure 21a shows that the residual impact vibration is obvious when the crack depth is 1.5 mm, 2 mm and 2.5 mm, and the vibration impact amplitude is approximately 3 g. Figure 21b shows that the residual increases with the deepening of the fault depth.

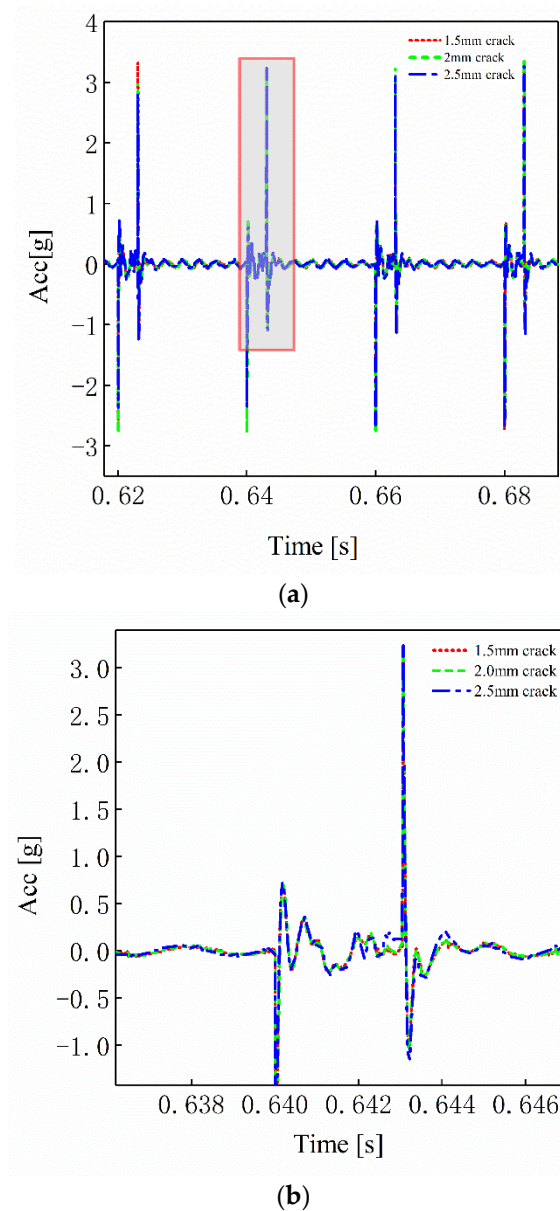


Figure 21. The residual signal of vibration acceleration with different crack depths. (a) The whole. (b) Zoomed plot.

With the increase of crack depth and crack angle, the amplitude of residual signal increases gradually. In order to diagnose the degree of crack fault more sensitively, statistical analysis of crack fault is needed.

6. Statistical Index Analysis of Time Domain Signal

The degree of crack failure can be evaluated by statistical indexes. The RMS, clearance factor, peak, crest factor, kurtosis, impulse factor, skewness, shape factor and other indicators of time-domain vibration signal are calculated, respectively, to evaluate the level of

crack failure. The calculation process of the above statistical indicators has been introduced in the literature [36], so we will not expand in detail here.

In order to reflect the degree of crack failure more sensitively, the method of percentage of statistical indicators is calculated. The percentage can be calculated as follows:

$$p_c = \frac{x_c - x_h}{x_h} * 100\% \quad (39)$$

where x_c is the value of statistical indicators in the faulty state, and x_h is the value of statistical indicators in the normal state.

The change of percentages of several statistical indexes when the crack angles increase is shown in Figure 22. As shown in the Figure 22, the skewness first decreases and then increases with the increase of the angle, and the difference is the largest at different angles among the statistical indexes. The impulse factor changes from 0 to -0.6% , which is second only to the skewness. The value of kurtosis changes from 0 to 0.31% as the angle increases from 0 to 60 degrees. The crest factor increases from 0 to 0.13% . The change of RMS is similar to the crest factor, whose value changes from 0 to approximately 0.1% . The shape factor and kurtosis factor change very slowly, almost close to 0, very insensitive to crack.

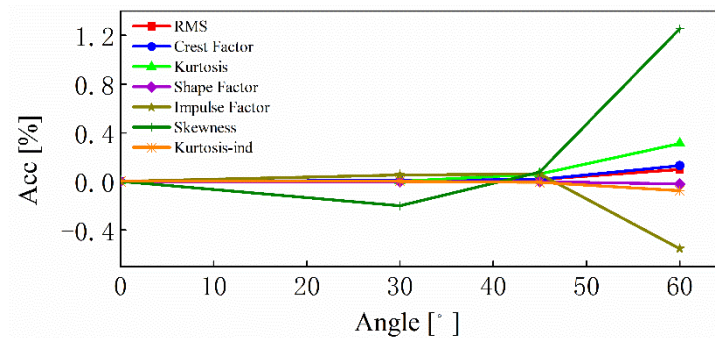


Figure 22. Change of percentage of statistical index with different crack angles.

Figure 23 is the percentage calculation result of these statistical indicators under different crack depths. Similar to the angle curve, the skewness is most sensitive to the change of crack depth. The impulse factor is also sensitive to crack, varying from 0 to approximately -0.55% . The change of kurtosis factor is weak, only from 0 to approximately -0.1% . The least obvious is the lower shape factor, whose change is almost zero.

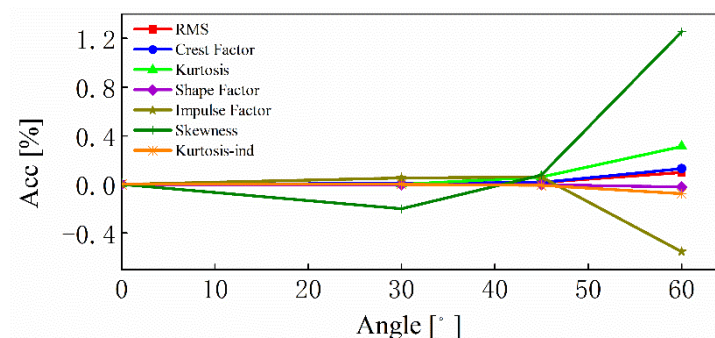


Figure 23. Variation of percentage of statistical index with different crack depths.

As can be seen from Figures 22 and 23, the gap between the statistical indicators and the normal condition becomes larger with the deepening of the fault degree. By comparing the percentages of the above statistical indexes at different crack angles and different crack depths, it is concluded that the skewness, impulse factor and kurtosis are more sensitive to the crack, and the sensitivity decreases in turn. It shows that the percentage of skewness can

be used as the judging basis for the crack evolution of the helical gear in the transmission system. The conclusion provides a basis for fault diagnosis of crack.

7. Conclusions and Future Work

To analyze the crack influence on two levels of helical gear transmission system, the meshing stiffness is improved. A two-stage dynamic model of the helical gear is established. The influence law of crack parameters on the vibration characteristics is analyzed. The sensitive degree of statistical indicators with a crack is studied in order to better implement the two-stage helical gear fault diagnosis. The following conclusions are drawn.

(1) Considering the axial force with crack fault, the stiffness decreases by 25%. The stiffness reduced more vigorously with the increase of crack depths and angles. The impact amplitude increases by 8.3%. The improved method is more helpful to crack fault diagnosis;

(2) There appears periodic interval under the faulty state in time domain. Sidebands appear around the mesh frequency and the harmonics of the first-stage gear pairs and the second-stage gear pairs, while there is a little influence on the vibration acceleration of the driven gear on the second-stage;

(3) The introduction of transmission error brings interference to the diagnosis of the crack fault. Residual signal can be more useful to diagnose the crack fault of the helical gear;

(4) According to the residual signals in frequency domain and time domain, we can tell by the gear which stage is cracked. While through the time required for the crack tooth from engagement to disengagement completely, we can tell which gear is cracked. we can tell the faulty gear pair of the two-stage helical gear transmission system, while through the impact periodic analysis, we can tell which gear is cracked. This is of great importance to the fault diagnosis in two-stage helical gear transmission system;

(5) The skewness, impulse factor and kurtosis change obviously to the crack fault, and their sensitivity decreases in turn. They can be used for the crack fault diagnosis of the helical gear.

The results proposed can be used for the crack diagnosis of helical gears. However, the dynamic characteristics and data processing method used in the electric transmission system need more efforts to investigate.

Author Contributions: Conceptualization, Y.L.; formal analysis, Y.L., W.W. and K.L.; funding acquisition, S.Y. and W.W.; investigation, Y.L.; methodology, Y.L.; project administration, Y.L.; resources, S.Y. and W.W.; supervision, W.W.; validation, Y.L. and C.L.; visualization, X.S.; writing—original draft, Y.L.; writing—review and editing, W.W., K.L. and X.S. All authors have read and agreed to the published version of the manuscript.

Funding: This work is supported by the National Natural Science Foundation of China (Grant no. U1864210).

Conflicts of Interest: The authors declare no conflict of interest.

Nomenclature

A_{x2}	the cross-sectional area at the coordinates, m^2
A_1	the abbreviation of an expression
b_{12}	the clearance between gear 1 and 2, m
b_{34}	the clearance between gear 3 and 4, m
C	the abbreviation of an expression
c_i	the torsional damping of drive shaft, $N/(m/s)$
c_{xi}	the bearing damp in the direction of x , $N/(m/s)$
c_{yi}	the bearing damp in direction of y , $N/(m/s)$
c_{zi}	the bearing damp in direction of z , $N/(m/s)$
d_a	the distance from the end point of the crack to the tooth root circle, m
d_k	the total meshing stiffness of wheelset slice unit, N/m
d_t	the distance from apex circle to root circle

e_{12}	the transmission error between gears 1 and 2, m
e_{34}	the transmission error between gears 3 and 4, m
E	the elasticity modulus, Pa
F	the meshing force, N
F_{12}	the contact force of gear 1 and 2 on the normal surface, N
F_{34}	the contact force of gear 3 and 4 on the normal surface, N
F_a	the axial force, N
f_{e3}	the rotation frequency of the output shaft, Hz
f_{m3}	the first gear mesh frequency, Hz
f_{m2}	the second gear mesh frequency, Hz
F_{y12}	the components of contact force of gear 1 and 2 along the end face, N
F_{z12}	the components of contact force of gear 1 and 2 in the axial direction, N
F_{y34}	the components of contact force of gear 3 and 4 along the end face, N
F_{z34}	the components of contact force of gear 3 and 4 in axial direction, N
g	the acceleration of gravity, $9.8 \text{ N} \cdot \text{kg}^{-1}$
G	the shear elasticity modulus, Pa
i	the number of the pair of gears engaged
k_b	the equivalent bending stiffness, N/m
k_s	the shearing stiffness, N/m
k_{rc}	the axial compression stiffness, N/m
k_{ab}	the axial bending stiffness, N/m
k_{as}	the axial shear stiffness, N/m
k_h	the Hertz contact stiffness, N/m
k_{xi}	the bearing stiffness in the direction of x for the gear i , N/m
k_{yi}	the bearing stiffness in the direction of y for the gear i , N/m
k_{zi}	the bearing stiffness in the direction of z for the gear i , N/m
L	the length of the contact line length, m
l_c	the depth of crack on the front, mm
N	the number of gears engaged at the same time
p_c	the percentage of statistical indicators
q	the crack length, mm
R_{b1}	the radius of the base cycle of the driving gear 1, m
R_{f1}	the radius of the root cycle of the driving gear 1, m
T	the rotation time of the gear in one cycle, s
t	the time, s
$t1$	the time one gear rotating from the tooth after the crack one, s
$t2$	the time the cracked tooth starts to enter mesh, s
$t3$	the time the tooth after the cracked tooth enters meshing, s
T_C	the time required for crack tooth rotating in one cycle, s
T_p	the input torque of the motor, N.m
T_g	the load torque, N.m
dU_b	the bending deformation energy of each slice, J
dU_s	the shear deformation energy of each slice, J
dU_{rc}	the axial compression deformation energy of each slice, J
dU_{ab}	the axial bending deformation energy of each slice, J
dU_{as}	the axial shear deformation energy of each slice, J
v	the passion ratio
x	the displacement in the x direction, m
x_2	the distance from meshing point to root circle, m
x_c	the value of statistical indicators in the fault state
x_h	the value of statistical indicators in the normal state
y	the displacement in the y direction, m
y_{12}	the normal vibration displacements along gears 1 and 2, m
y_{34}	the normal vibration displacements along gears 3 and 4, m
z	the displacement in the z direction, m

Greeks

α_n	the normal pressure angle, rad
α_t	the end pressure angle of the helical gear, rad
γ	the crack angle on the end face, rad
p	the driving gear
g	the driven gear
β	the helical gear helix angle, rad
θ	the torsional vibration, deg.

Abbreviations

RMS the root-mean-square value

References

1. Wu, G.; Wu, H.; Li, D. Review of Automotive Transmission Gear Rattle. *J. Tongji Univ.* **2016**, *44*, 276–285.
2. Spitas, C.; Spitas, V. Coupled multi-DOF dynamic contact analysis model for the simulation of intermittent gear tooth contacts, impacts and rattling considering backlash and variable torque. *Proc. Inst. Mech. Eng. Part C J. Mech. Eng. Sci.* **2016**, *230*, 1022–1047. [[CrossRef](#)]
3. Yang, D.C.H.; Lin, J.Y. Hertzian damping, tooth friction and bending elasticity in gear impact dynamics. *J. Mech. Transm. Autom. Des.* **1987**, *109*, 189–196. [[CrossRef](#)]
4. Tian, X. Dynamic Simulation for System Response of Gearbox Including Localized Gear Faults. Master's Thesis, Albert University, Edmonton, AB, Canada, 2004.
5. Sainsot, P.; Velex, P. Contribution of gear body to tooth deflections—A new bidimensional analytical formula. *Trans. ASME* **2004**, *126*, 748–752. [[CrossRef](#)]
6. Wan, Z.; Cao, H.; Zi, Y.; He, W.; He, Z. An improved time-varying mesh stiffness algorithm and dynamic modeling of gear-rotor system with tooth root crack. *Eng. Fail. Anal.* **2014**, *42*, 157–177. [[CrossRef](#)]
7. Ma, H.; Song, R.; Pang, X.; Wen, B. Time-varying mesh stiffness calculation of cracked spur gears. *Eng. Fail. Anal.* **2014**, *44*, 179–194. [[CrossRef](#)]
8. Wang, Q.; Zhao, B.; Fu, Y.; Kong, X.; Ma, H. An improved time-varying mesh stiffness model for helical gear pairs considering axial mesh force component. *Mech. Syst. Signal Process.* **2018**, *106*, 413–429. [[CrossRef](#)]
9. Jiang, H.; Liu, F. Mesh stiffness modelling and dynamic simulation of helical gears with tooth crack propagation. *Meccanica* **2020**, *55*, 1215–1236. [[CrossRef](#)]
10. Wang, S.; Zhu, R. An improved mesh stiffness calculation model for cracked helical gear pair with spatial crack propagation path. *Mech. Syst. Signal Process.* **2022**, *172*, 108989. [[CrossRef](#)]
11. Wang, S.; Zhu, R. An improved mesh stiffness model of helical gear pair considering axial mesh force and friction force influenced by surface roughness under EHL condition. *Appl. Math. Model.* **2022**, *102*, 453–471. [[CrossRef](#)]
12. Wang, S.; Zhu, R.; Xiao, Z. Investigation on crack failure of helical gear system of the gearbox in wind turbine: Mesh stiffness calculation and vibration characteristics recognition. *Ocean. Eng.* **2022**, *250*, 110971–110972. [[CrossRef](#)]
13. Yan, H.; Wen, L.; Yin, S.; Cao, H.; Chang, L. Research on gear mesh stiffness of helical gear based on combining contact line analysis method. *J. Mech. Eng. Sci.* **2022**, *236*, 9354–9366. [[CrossRef](#)]
14. Zhang, C.; Dong, H.; Wang, D.; Dong, B. A new effective mesh stiffness calculation method with accurate contact deformation model for spur and helical gear pairs. *Mech. Mach. Theory* **2022**, *171*, 104762. [[CrossRef](#)]
15. Yang, H.; Shi, W.; Chen, Z.; Guo, N. An improved analytical method for mesh stiffness calculation of helical gear pair considering time-varying backlash. *Mech. Syst. Signal Process.* **2022**, *170*, 108882. [[CrossRef](#)]
16. Huangfu, Y.; Chen, K.; Ma, H.; Che, L.; Li, Z. Deformation and meshing stiffness analysis of cracked helical gear pairs. *Eng. Fail. Anal.* **2019**, *95*, 30–46. [[CrossRef](#)]
17. Huangfu, Y.; Chen, K.; Ma, H.; Li, X.; Han, H.; Zhao, Z. Meshing and dynamic characteristics analysis of spalled gear systems: A theoretical and experimental study. *Mech. Syst. Signal Process.* **2020**, *139*, 106640–106661. [[CrossRef](#)]
18. Lin, T.; Guo, S.; Zhao, Z. Influence of crack faults on time-varying mesh stiffness and vibration response of helical gears. *J. Vib. Shock.* **2019**, *38*, 29–36.
19. Tuplin, W.A. Gear-tooth stresses at high speed. *Proc. Inst. Mech. Eng.* **1950**, *163*, 162–175. [[CrossRef](#)]
20. Kahraman, A.; Singh, R. Interactions between time-varying mesh stiffness and clearance non-linearities in a geared system. *J. Sound Vib.* **1991**, *146*, 135–156. [[CrossRef](#)]
21. Brethee, K.F.; Zhen, D.; Gu, F.; Ball, A.D. Helical gear wear monitoring: Modelling and experimental validation. *Mech. Mach. Theory* **2017**, *117*, 210–229. [[CrossRef](#)]
22. Chen, Z.; Zhai, W.; Wang, K. Vibration feature evolution of locomotive with tooth root crack propagation of gear transmission system. *Mech. Syst. Signal Process.* **2019**, *115*, 29–44. [[CrossRef](#)]

23. Meng, Z.; Shi, G.; Wang, F. Vibration response and fault characteristics analysis of gear based on time-varying mesh stiffness. *Mech. Mach. Theory* **2020**, *148*, 103786–103801. [[CrossRef](#)]
24. Chen, C. Dynamic Modeling of Two-Stage Planetary Gearbox with Tooth Cracks and Its Dynamic Response Analyses. Master's Thesis, University of Electronic Science and Technology of China, Chengdu, China, 2017.
25. Wei, C.; Wu, W.; Hou, X.; Yuan, S. Study on Oil Distribution and Oil Content of Oil Bath Lubrication Bearings Based on MPS Method. *Tribol. Trans.* **2022**, *65*, 942–951. [[CrossRef](#)]
26. Spitas, C.; Spitas, V. Calculation of overloads induced by indexing errors in spur gearboxes using multi-degree-of-freedom dynamical simulation. *Proc. Inst. Mech. Eng. Part K J. Multi-Body Dyn.* **2006**, *220*, 273–282. [[CrossRef](#)]
27. Shehata, A.; Adnan, M.A.; Mohammed, O.D. Modeling the effect of misalignment and tooth microgeometry on helical gear pair in mesh. *Eng. Fail. Anal.* **2019**, *106*, 104190. [[CrossRef](#)]
28. Sakaridis, E.; Spitas, V.; Spitas, C. Non-linear modeling of gear drive dynamics incorporating intermittent tooth contact analysis and tooth eigenvibrations. *Mech. Mach. Theory* **2019**, *136*, 307–333. [[CrossRef](#)]
29. Wang, Q.; Ma, H.; Kong, X.; Zhang, Y. A distributed dynamic mesh model of a helical gear pair with tooth profile errors. *J. Cent. South Univ.* **2018**, *25*, 287–303. [[CrossRef](#)]
30. Yan, P.; Liu, H.; Gao, P.; Zhang, X.; Zhan, Z.; Zhang, C. Optimization of distributed axial dynamic modification based on the dynamic characteristics of a helical gear pair and a test verification. *Mech. Mach. Theory* **2021**, *163*, 104371. [[CrossRef](#)]
31. Jiang, H.; Liu, F. Dynamic characteristics of helical gears incorporating the effects of coupled sliding friction. *Meccanica* **2022**, *57*, 523–539. [[CrossRef](#)]
32. Wei, P.; Deng, S. Time-varying Mesh Stiffness Calculation and Research on Dynamic Characteristic of Two-stage Helical Gear System based on Potential Energy Method. *Jixie Chuangdong* **2020**, *44*, 51–57.
33. Liu, J.; Zhao, W.; Liu, W. Frequency and Vibration Characteristics of High-Speed Gear-Rotor-Bearing System with Tooth Root Crack considering Compound Dynamic Backlash. *Shock. Vib.* **2019**, *2019*, 1854263. [[CrossRef](#)]
34. Sun, G.; Zhao, S. *Mechanics of Materials*; Shanghai Jiaotong University Press: Shanghai, China, 2006.
35. Zhu, X. *Handbook of Gear Design*; Chemical Industry Press: Beijing, China, 2004.
36. Sharma, V.; Parey, A. A Review of Gear Fault Diagnosis Using Various Condition Indicators. *Procedia Eng.* **2016**, *144*, 253–263. [[CrossRef](#)]